Free energy model for hysteresis in magnetostrictive transducers

Ralph C. Smith[a)]
Department of Mathematics, Center for Research in Scientific Computation,
North Carolina State University, Raleigh, North Carolina 27695

Marcelo J. Dapino
Department of Mechanical Engineering, The Ohio State University, Columbus, Ohio 43210

Stefan Seelecke
Mechanical and Aerospace Engineering, Center for Research in Scientific Computation, North Carolina
State University, Raleigh, North Carolina 27695

This article addresses the development of a free energy model for magnetostrictive transducers operating in hysteretic and nonlinear regimes. Such models are required both for material and system characterization and for model-based control design. The model is constructed in two steps. In the first, Helmholtz and Gibbs free energy relations are constructed for homogeneous materials with constant internal fields. In the second step, the effects of material nonhomogeneities and nonconstant effective fields are incorporated through the construction of appropriate stochastic distributions. Properties of the model are illustrated through comparison and prediction of data collected from a typical Terfenol-*D* transducer.   © *2003 American Institute of Physics.*
[DOI: 10.1063/1.1524312]

I. INTRODUCTION

Magnetostrictive transducers are being considered for a number of high performance industrial, automotive, biomedical and Department of Defense applications due to their capability for generating large force inputs over a broad frequency range. As detailed in Refs. 1–3, applications utilizing magnetostrictive transducers include, among others, active vibration and noise control, micropositioning in high force regimes, medical and industrial ultrasonics, noncontact torque sensors, and tuned vibration absorbers. As the field of magnetostrictive materials becomes more mature, it is anticipated that a growing number of actuator and sensor applications will benefit from the multifunctional characteristics and robust operation that these materials can provide.

An inherent property of all existing magnetostrictive materials, however, is the presence of hysteresis and constitutive nonlinearities in the relation between input fields and the generated magnetization and strains as illustrated in Fig. 1. While the effects of hysteresis and nonlinearities can be reduced through the choice of stoichiometry[4] and feedback mechanisms, the modeling of these effects in a manner compatible with subsequent control design can yield significant improvements in performance.

To illustrate issues pertinent to model development and control design for a typical magnetostrictive transducer, we consider the device depicted in Fig. 2. Input to the system is provided by a current $I(t)$ applied to the solenoid which generates a field $H(t)$. This causes magnetic moments in the Terfenol-*D* rod to rotate which produces the strains and stresses output by the device. The prestress mechanisms serve two purposes: they further align magnetic moments to improve performance and they maintain the Terfenol rod in a state of compression. The surrounding permanent magnet provides a bias field H_0 necessary to achieve bidirectional strains and can also be designed to optimize flux paths through the rod. The hysteretic data plotted in Fig. 1 are typical of this type of Terfenol-*D* transducer and hence they represent criteria that must be accommodated in models to be employed for design, analysis and control development.

A number of techniques have been considered for quantifying the hysteresis and constitutive nonlinearities inherent to the relation between input field H and the magnetization M and strain e generated. For Terfenol-*D* transducers, these include Preisach models[5,6] and domain wall models[7–9] based on the magnetic theory of Jiles and Atherton.[10,11] For transducer characterization and control design, crucial requirements for the models include automatic closure of biased minor loops, flexibility with regard to temperature and frequency, and sufficient efficiency to permit real-time implementation. The Preisach techniques guarantee minor loop closure but require a large number of nonphysical parameters for accurate biased minor loop characterization. Furthermore, modifications to classical Preisach theory are required to accommodate temperature dependence, reversible changes in the magnetization observed at low drive levels, or to relax congruency requirements to ensure that minor loops remain inside major loops.[12,13] This limits the feasibility of control techniques based on Preisach models to a limited number of applications. Conversely, the physical basis for domain wall models makes them applicable to a broader performance space. However, although techniques have been developed to guarantee closure of biased minor loops when turning points are known *a priori*,[14,15] the closure of minor loops when these points are not know *a priori*, as will be the case in closed loop feedback design, is not guaranteed by present domain wall models. This proves a serious detriment in control design.
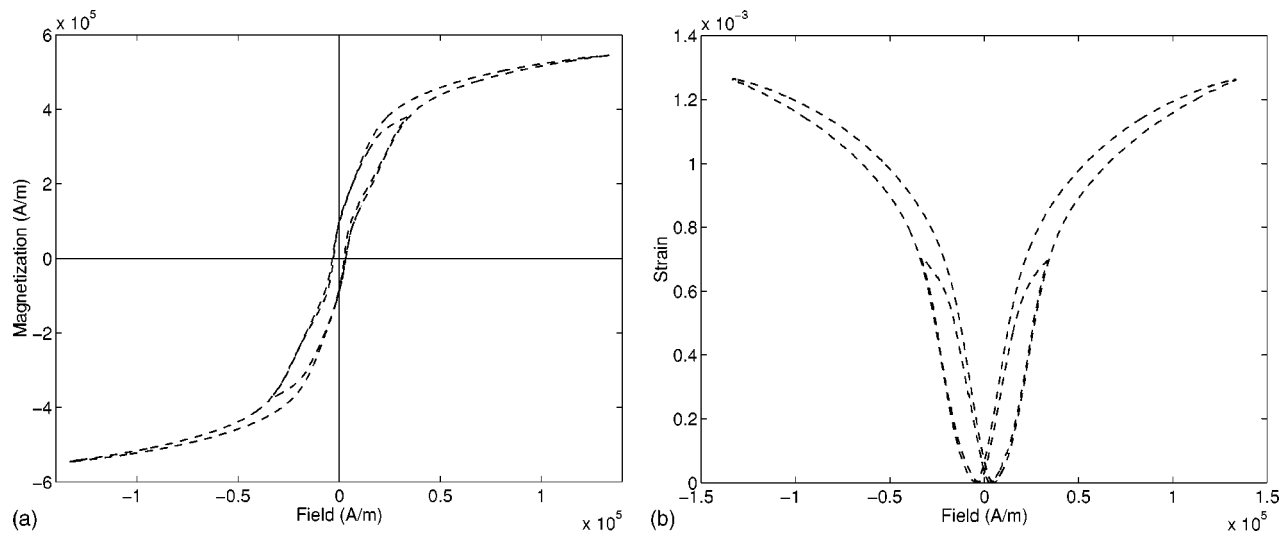
---

a)Electronic mail: rsmith@eos.ncsu.edu

FIG. 1. Hysteretic data measured in a Terfenol-*D* transducer of the (a) field-magnetization relation and (b) field-strain relation (from Ref. 8).

In this article, we quantify hysteresis and constitutive nonlinearities inherent to Terfenol-*D* magnetostrictive transducers through the development of a free energy model. In the first step of the development, we derive appropriate relations for the Helmholtz and Gibbs free energies at the lattice or domain level. This yields a local magnetization model for homogeneous, single crystal materials. The effects of material nonhomogeneities and nonuniform effective fields are then incorporated through consideration of stochastic distributions. This yields a macroscopic model which quantifies the hysteretic relation between H and M. A more general free energy relation that includes magnetoelastic interactions is then employed to develop nonlinear constitutive relations which predict the nonlinear relation between fields H and strains ε.

The model quantifies hysteresis in the relations between H and M and H and ε for temperature invariant and quasi-static operating conditions. Although certain relaxation mechanisms are included, the model presently neglects eddy current losses and hence it should be employed for low frequency regimes. Furthermore, the model is developed for transducer configurations in which prestress levels are sufficiently high that they dominate crystalline anisotropies and thus, in this initial development, anisotropy energy is neglected. Finally, it is illustrated that the model ensures the closure of biased, nested minor loops in both the $H-M$ and $H-\varepsilon$ relations.

The nonlinear magnetization model is developed in Secs. II B and II C and the full constitutive relations are developed in Sec. II D. The accuracy of the model is illustrated in Sec. III through comparison and prediction of data collected from a typical Terfenol-*D* transducer. The capability of the model to ensure closure of biased minor loops is illustrated through a numerical example.

II. MODEL DEVELOPMENT

To motivate the development of a hysteresis model for Terfenol-*D*, we summarize first pertinent properties of its crystalline structure. This is facilitated by vector conventions in which planes are denoted by round brackets and directional indices are represented by square brackets. Hence the faces of a cube are denoted by $(100),(010),(001),$ $(\bar{1}00),(0\bar{1}0),(00\bar{1})$ whereas the vertices are specified by $[100],[010],[001],[\bar{1}00],[0\bar{1}0],[00\bar{1}]$. In both cases, $\bar{1}$, indicates a negative direction. Finally, angular brackets are used to summarize an entire set of indices.

In present manufacturing processes, Terfenol-*D* crystals are grown in dendrite sheets oriented in the $[11\bar{2}]$ direction as depicted in Fig. 3. At room temperature, the easy axes lie approximately in the $\langle 111 \rangle$ set of directions and the greatest strains occur when the magnetization M rotates from $[111]$ to $[11\bar{1}]$.
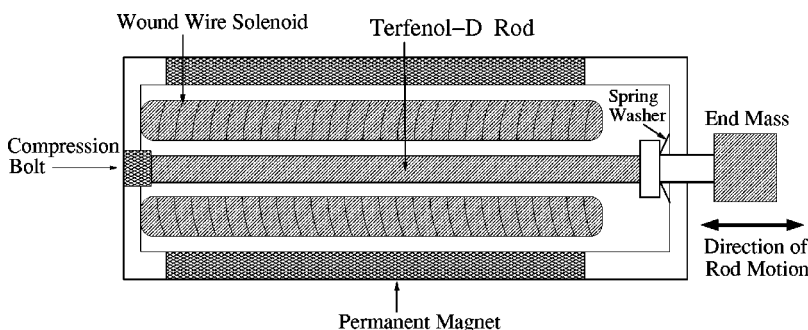

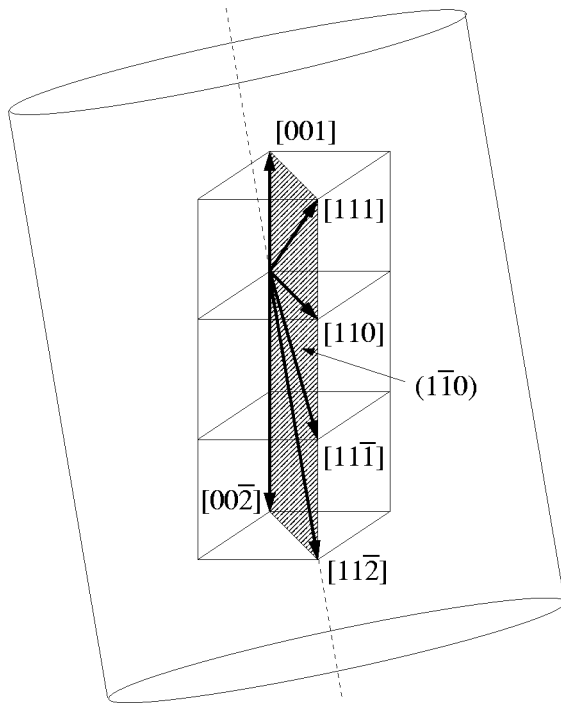FIG. 2. Cross section of a typical Terfenol-*D* magnetostrictive transducer.

FIG. 3. Orientation of Terfenol-*D* crystals.

The changes in magnetism that result from an applied field H are primarily due to two mechanisms: the rotation of moments and the movement of domain walls. To illustrate, consider a demagnetized specimen which is subjected to a magnetic field oriented in the $[11\bar{2}]$ direction as shown in Fig. 4. At low field levels, the change in magnetization is due primarily to domain wall motion so that favorably oriented domains are enlarged. As the field is increased, moments rotate to orient with the easy $[11\bar{1}]$ axis. This produces a burst region in the $H-M$ or $H-\varepsilon$ curve in which small changes in field produce large changes in magnetization or strain. In the final stage depicted in Fig. 4(d), the material acts as a single domain as moments rotate coherently from the easy axis into the direction of the field applied. This produces the saturation behavior exhibited by the material.

Strains are generated by the material when moments rotate to align with an applied field. For general configurations, the magnetomechanical coupling which produces these

strains is highly complex and dependent upon factors such as the stress applied and crystalline anisotropies. However, in the case of materials in which prestress perpendicular to the moment direction is sufficiently large to dominate crystalline anisotropy, the preferred orientation of domains is shifted from the original eight $\langle 111 \rangle$ magnetic easy axes to the two axes $[111]$ and $[\bar{1}\bar{1}1]$ perpendicular to the $[11\bar{2}]$ direction. In this regime, strains are due primarily to moment rotation and the free strain, or magnetostriction, can be modeled by the quadratic relation

$$\lambda = \frac{3}{2}\lambda_s \left(\frac{M}{M_s}\right)^2, \tag{1}$$

where λ_s and M_s, respectively, denote the saturation magnetostriction and magnetization. As discussed in Refs. 7 and 10, the prestress levels needed to optimize transducer performance are often of such magnitude such that stress anisotropy dominates crystalline anisotropy and relation (1) adequately models the strain generated by the material.

To model the hysteretic behavior of the material, we first quantify the nonlinear relation between input fields H and magnetization M. We then develop constitutive relations that incorporate the quadratic behavior, Eq. (1), to provide an initial model for the strain produced by the transducer.

A. Thermodynamic preliminaries

To provide a common framework for constructing magnetostatic and magnetoelastic energy relations, we consider general properties of free energy relations. The free energy is assumed to be a function of temperature T and an order parameter e which is respectively taken to be the magnetization M in magnetostatic relations and the strain ε in magnetoelastic relations. We let $\tilde{\phi}$ denote external fields that are thermodynamically conjugate to e. For the order parameters M and ε, appropriate choices for the external field $\tilde{\phi}$ are the magnetic field H and stress σ. Finally, we let $\psi(e,T)$ denote a general Helmholtz free energy relation.

In the absence of applied fields, thermodynamic equilibria are determined by minimizing ψ with respect to e which, under the assumption of differentiability, yields the necessary condition,
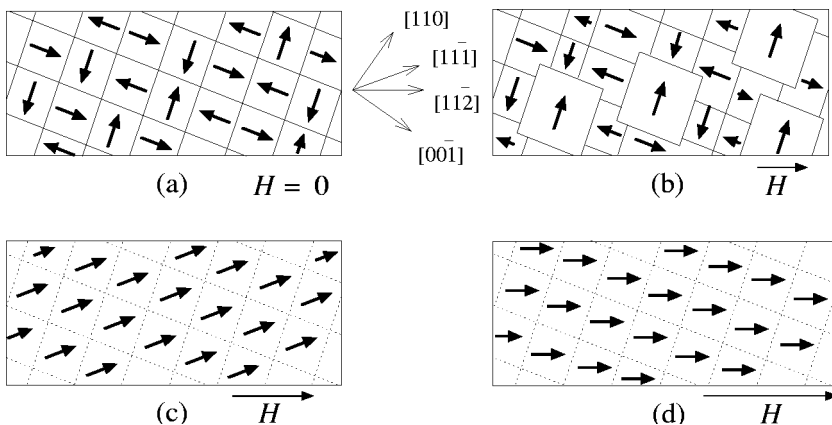

FIG. 4. Magnetization process in the $(1\bar{1}0)$ plane of single crystal Terfenol-*D* due to field H applied in the $[11\bar{2}]$ direction. (a) Demagnetized state and (b) growth of domains due to domain wall motion. (c) Rotation of moments to the easy $[11\bar{1}]$ axis, and (d) rotation of moments to align with the applied field.

$$\phi(e,T) \equiv \frac{\partial \psi}{\partial e} = 0,$$

where ϕ denotes the energetic response of the system. For systems subjected to an external field $\tilde{\phi}$, the total free energy is taken to be

$$\psi_{\tilde{\phi}}(e,T) = \psi(e,T) - \tilde{\phi}e, \tag{2}$$

which yields the equilibrium condition

$$\phi(e,T) = \tilde{\phi}. \tag{3}$$

Relation (3) can be physically interpreted as providing conditions under which the order parameter adjusts to balance the internal energy with that of the external field. As will be illustrated later, relation (3) also provides the constraints used to specify effective fields as well as magnetoelastic constitutive relations.

B. Magnetic hysteresis model

Motivated by the prestressed operating regime which yields the $[111]$ and $[\overline{1}11]$ easy magnetic axes, we now consider the energy of a magnetic moment with two preferred orientations. This includes characterization of the internal and magnetostatic energy. Magnetoelastic interactions are included in Sec. II D and used to develop elastic constitutive relations.

We first formulate a Helmholtz potential ψ by considering internal energy contributions due to moment interactions. These interactions are assumed to be isothermal and hence temperatures in all subsequent expressions are assumed to be fixed below the Curie point, which implies that the material under study is in its ferromagnetic phase. This condition, when combined with the assumption that stress anisotropy dominates crystalline anisotropy, yields material behavior consistent with a double well potential of the form illustrated in Fig. 5. As summarized in Ref. 16, statistical mechanics analysis determines that, at fixed temperatures, a first-order approximation to the potential exhibits quadratic behavior in the neighborhoods of all three equilibria. Hence we employ the piecewise quadratic definition,

$$\psi(M) = \begin{cases} \dfrac{1}{2}\eta(M+M_R)^2, & M \leq -M_I, \\[2mm] \dfrac{1}{2}\eta(M-M_R)^2, & M \geq M_I, \\[2mm] \dfrac{1}{2}\eta(M_I-M_R)\left(\dfrac{M^2}{M_I}-M_R\right), & |M|<M_I, \end{cases} \tag{4}$$

for the Helmholtz free energy. As illustrated in Fig. 5(a), M_I and M_R, respectively, denote the inflection point and magnetization at which the minimum of ψ occurs.

From Eq. (2), the Gibbs energy is taken to be

$$G = \psi - HM, \tag{5}$$

which, for increasing field H, is illustrated in Fig. 5(a). Since the magnetostatic energy is given by $\mathcal{E} = \mu_0 MH$, where μ_0 is the magnetic permeability, a second choice for the Gibbs
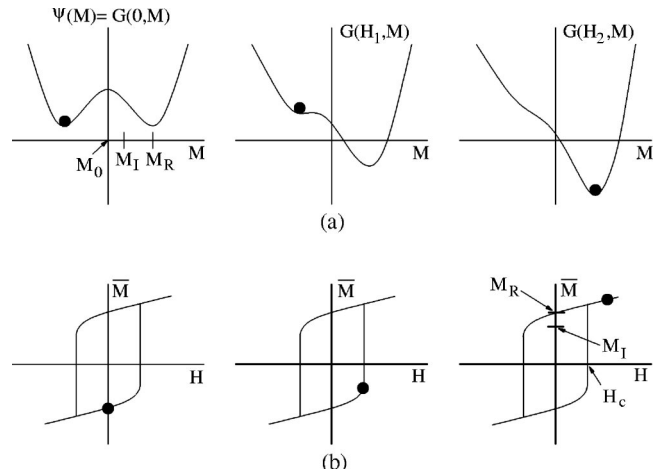

FIG. 5. (a) Helmholtz energy ψ and Gibbs energy G for increasing field H ($H_2 > H_1 > 0$). (b) Local magnetization $\bar{M}$ as a function of H for a homogeneous, isotropic material.

energy is $G = \psi - \mu_0 HM$. However, because formulation (5) can be viewed as incorporating μ_0 into ψ, the two energy formulations yield equivalent final models, and we employ formulation (5) for simplicity.

For a homogeneous material with effective field $H_e = H$, where H denotes the field applied, the average local magnetization is given by

$$\bar{M} = x_+\langle M_+\rangle + x_-\langle M_-\rangle, \tag{6}$$

where x_+ and x_-, respectively, denote the fraction of moments having positive and negative orientations, and $\langle M_+\rangle$ and $\langle M_-\rangle$ are the expected values of the resulting magnetizations. To specify $\langle M_+\rangle$, we take

$$\langle M_+\rangle = \int_{M_0}^{\infty} M\mu(G)dM, \tag{7}$$

where

$$\mu(G) = Ce^{-GV/kT} \tag{8}$$

quantifies the probability of obtaining the energy level G, k is the Boltzmann constant, C denotes a constant chosen to yield a probability of 1 for integration over all possible magnetization values, and M_0 is the critical point that corresponds to the unstable equilibrium. The Boltzmann energy balance is considered over a lattice volume V chosen to yield relaxation behavior appropriate for the material being characterized. Subsequent evaluation of C yields the average magnetization values,

$$\langle M_+\rangle = \frac{\int_{M_0}^{\infty} M e^{-G(H,M)V/kT}dM}{\int_{M_0}^{\infty} e^{-G(H,M)V/kT}dM},$$

$$\langle M_-\rangle = \frac{\int_{-\infty}^{M_0} M e^{-G(H,M)V/kT}dM}{\int_{-\infty}^{M_0} e^{-G(H,M)V/kT}dM}. \tag{9}$$

We note that, when implementing the model, we typically replace M_0 by the inflection points M_I and $-M_I$, respectively, in the relations for $\langle M_+\rangle$ and $\langle M_-\rangle$. This simplifies approximation of the integrals and can be motivated by
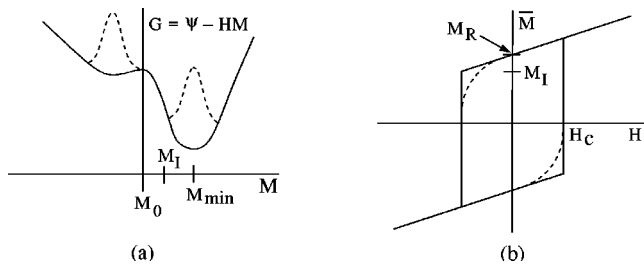
FIG. 6. (a) Gibbs energy profile with a high level of thermal activation $(- - -)$ in the Boltzmann probability $\mu(G) = Ce^{-GV/kT}$. (b) Local magnetization $\bar{M}$ given by Eq. (6) with high thermal activation $(- - -)$ and limiting magnetization $\bar{M}$ specified by Eq. (12) in the absence of thermal activation (——).

observing that, if one considers the forces $\partial G/\partial M$ due to the field applied, maximum restoring forces occur at M_I and $-M_I$ (e.g., see pages 332–333 of Ref. 17). Furthermore, for materials with low thermal activation, points M_0 and $-M_I$ coincide in the limit as thermal activation is reduced to zero for positive fields while M_I and M_0 coincide for negative fields as illustrated in Fig. 6.

The moment fractions x_+ and x_- are quantified by the evolution equations,

$$\dot{x}_+ = -p_{+-}x_+ + p_{-+}x_- ,$$

$$\dot{x}_- = -p_{-+}x_- + p_{+-}x_+ ,$$

which can be simplified to

$$\dot{x}_+ = -p_{+-}x_+ + p_{-+}(1-x_+) \tag{10}$$

through the identity $x_+ + x_- = 1$. The likelihoods of switching orientations are specified by

$$p_{+-} = \sqrt{\frac{kT}{2\pi m V^{2/3}}} \frac{e^{-G(H,M_I)V/kT}}{\int_{M_I}^{\infty} e^{-G(H,M)V/kT}dM},$$

$$p_{-+} = \sqrt{\frac{kT}{2\pi m V^{2/3}}} \frac{e^{-G(H,-M_I)V/kT}}{\int_{-\infty}^{-M_I} e^{-G(H,M)V/kT}dM}, \tag{11}$$

where m is the mass of lattice volume V.

Because expression (6) for the local magnetization $\bar{M}$ is probabilistic in the sense that the moment rotations are determined by Eq. (8), the map between the field and magnetization exhibits both hysteresis and nonlinear transition behavior as depicted in Fig. 5(b). The degree to which the transition is mollified is dependent on the ratio between GV and kT in the Boltzmann relation [Eq. (8)]; large values of kT model regimes in which thermal activation is prominent. This in turn yields smoother transitions since, for a fixed field level, moments have a higher probability of achieving the thermal energy required to overcome energy barriers.

The complex behavior of $\bar{M}$ can be simplified in two aspects to facilitate both qualitative analysis of the model and its quantitative implementation for regimes in which thermal activation is negligible. The qualitative behavior can be ascertained by analyzing the equilibrium behavior after moments have switched. In this regime, the equilibrium con-

dition $\partial G/\partial M = 0$ yields $H = \partial \psi/\partial M$. Hence the local model predicts a linear relation between H and $\bar{M}$ after moment switching. Furthermore, from $\partial H/\partial M = \partial^2 \psi/\partial M^2$, it follows that the slope of the hysteresis kernel in this linear regime is $1/\eta$. The correspondence between the critical point M_R and remanence behavior of a homogeneous single crystal follows directly from the zero field behavior of the Gibbs energy. The transition point occurs at inflection point M_I since this is the point of maximum restoring force.[17] In concert, these equilibrium conditions yield criteria which can be employed to determine initial parameter values for optimization routines used to estimate parameters in the final transducer models.

For regimes in which operating time scales make thermal activation negligible, asymptotic relations can be employed to simplify the magnetization relations since jumps in this case can be considered to occur instantaneously as depicted in Fig. 6. In this regime, $\bar{M} = M_{\min}$ where $M_{\min}$ is obtained through the solution of $\partial G/\partial M = 0$. For the quadratic Helmholtz model [Eq. (4)], the local magnetization in this limiting case is given by

$$[\bar{M}(H;H_c,\xi)](t)$$

$$= \begin{cases} [\bar{M}(H;H_c,\xi)](0), & \tau(t)=\varnothing, \\ \dfrac{H}{\eta}-M_R, & \tau(t)\neq\varnothing \ \text{and} \ H[\max\tau(t)]=-H_c, \\ \dfrac{H}{\eta}+M_R, & \tau(t)\neq\varnothing \ \text{and} \ H[\max\tau(t)]=H_c, \end{cases}$$

$$\tag{12}$$

where $[\bar{M}(H;H_c,\xi)](0)$ denotes the initial moment orientation and transition points are specified by

$$\tau(t) = \{t \in (0,T_f) \,|\, H(t)=-H_c \ \text{or} \ H(t)=H_c\}. \tag{13}$$

Employing the notation used for Preisach models,[18] the initial moment orientation is specified by

$$[\bar{M}(H;H_c,\xi)](0) = \begin{cases} \dfrac{H}{\eta}-M_R, & H(0)\leqslant -H_c, \\ \xi, & -H_c<H(0)<H_c, \\ \dfrac{H}{\eta}+M_R, & H(0)\geqslant H_c. \end{cases}$$

$$\tag{14}$$

The dependence of $\bar{M}$ on the local coercive field $H_c \equiv \eta(M_R-M_I)$ is explicitly indicated since parameter η is considered to be distributed for the bulk model developed in Sec. II C.

C. Nonhomogeneous materials and effective fields

The local magnetization models [Eqs. (6) or (12)] are derived under the assumption that the lattice and hence domain structure in the materials is completely homogeneous so that free energy profiles for different regions in the material are identical. However, this typically is not the case due to material defects, nonuniformities in the crystalline structure, and polycrystallinity. Furthermore, the models assume
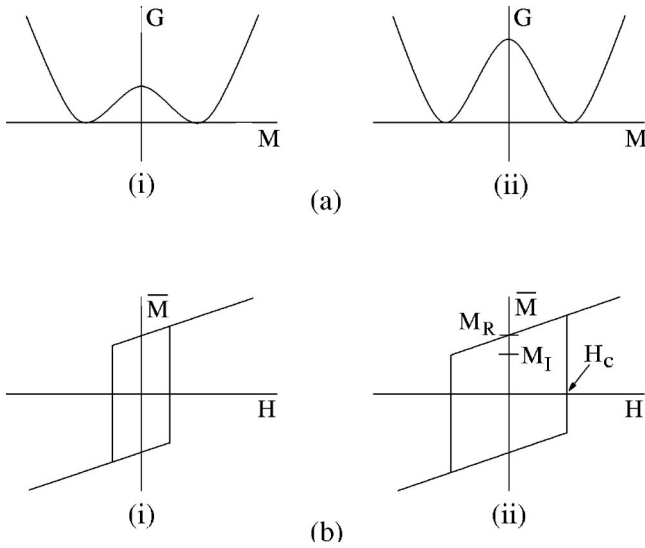
FIG. 7. (a) Free energies associated with nonuniform moment distributions. (b) Variations in the local coercive field H_c for the hysteresis kernel due to differing free energies.

that the effective field H_e at the domain level is exactly the field H applied and hence they ignore magnetic interactions or Weiss field effects. Through the incorporation of appropriate stochastic distributions, we extend the local model to obtain a bulk magnetization model for nonhomogeneous materials with nonconstant effective fields.

To accommodate general material nonhomogeneities, we assume that materials exhibit a distribution of free energy profiles which produce variations in the width of the hysteresis kernels predicted by Eqs. (6) or (12) as depicted in Fig. 7. Nonhomogeneities are incorporated by assuming that parameters M_R, M_I, or $H_c = \eta(M_R - M_I)$ are manifestations of an underlying distribution rather than constants as assumed in Sec. II B. For this initial model, we consider H_c to be normally distributed with mean $\bar{H}_c$. In this case, the total magnetization is given by

$$M(H) = \int_0^\infty \bar{M}(H;H_c,\xi) f(H_c) dH_c, \tag{15}$$

with the density

$$f(H_c) = C_1 e^{-(H_c - \bar{H}_c)^2/b}. \tag{16}$$

Here, C_1 and b are positive parameters and $\bar{M}$ is specified by Eqs. (6) or (12). We note that in Eq. (15), the lower limit of 0 reflects the requirement that hysteresis kernels have nonnegative width. Alternatively, f can be specified as a log–normal density to reflect the positivity of the kernel widths.

The second extension addresses the incorporation of mean field effects due to interdomain coupling. In the models of Jiles and Atherton[10,11] and in subsequent magnetostrictive transducer models,[7–9] this coupling was modeled by an effective field of the form

$$H_e = H + \alpha M, \tag{17}$$

where α is a constant mean field parameter. The effective field [Eq. (17)] is analogous to the Weiss mean field which quantifies interatomic interactions. Rather than assume a constant interaction coefficient α, we assume that the effective field can exhibit variations due to nonhomogeneities in the distribution of magnetic moments. To incorporate these field variations, we consider the effective field to be normally distributed about the field applied. For fixed H_c, the magnetization in this case is given by

$$M(H) = \int_{-\infty}^\infty C_2 \bar{M}(\mathcal{H};H_c,\xi) e^{-(H-\mathcal{H})^2/\bar{b}} d\mathcal{H}. \tag{18}$$

The variations in the effective field produce domain switching in advance of the remanence point in accordance with observations from experimental data.

The full magnetization model for nonhomogeneous polycrystalline materials with variable effective fields then becomes

$$[M(H)](t) = C \int_0^\infty \int_{-\infty}^\infty [\bar{M}(\mathcal{H}+H,H_c,\xi)](t)$$
$$\times e^{-\mathcal{H}^2/\bar{b}} e^{-(H_c - \bar{H}_c)^2/b} d\mathcal{H} dH_c, \tag{19}$$

with $\bar{M}$ again given by Eqs. (6) or (12). We note that for implementation purposes, the integrals are truncated using high-order Gaussian quadrature to achieve low-order systems which facilitate efficient implementation.

Although the model [Eq. (19)] does incorporate certain relaxation mechanisms, it does not yet incorporate eddy current losses so its use should be restricted to low frequency drive regimes. The inclusion of eddy current losses and variable temperature operating regimes to accommodate ohmic heating can be addressed by including appropriate terms in the energy relations.

D. Magnetoelastic constitutive relations

The Gibbs relation [Eq. (5)] incorporates the internal energy and magnetostatic energy exhibited by isotropic materials at the domain level. However, it neglects the magnetoelastic coupling which provides the materials with magnetostrictive capabilities. Motivated by experimental evidence that suggests a quadratic dependence of strain on the magnetization, we consider the magnetostrictive relation (1). Although this relation is customarily employed in magnetostrictive transducer design due to its simplicity, it can only be justified theoretically in applications where material stresses are such that stress anisotropy overwhelms crystalline anisotropy. In this case, magnetoelastic coupling can be incorporated through consideration of the magnetoelastic Helmholtz free energy relation

$$\psi_e(M,\varepsilon) = \psi(M) + \tfrac{1}{2} Y^M \varepsilon^2 - Y^M \gamma \varepsilon M^2, \tag{20}$$

and corresponding Gibbs energy,

$$G(H,M,\varepsilon) = \psi(M) + \tfrac{1}{2} Y^M \varepsilon^2 - Y^M \gamma \varepsilon M^2 - HM - \sigma\varepsilon, \tag{21}$$

where ψ is specified by Eq. (4). Here Y^M denotes the

Young's modulus at constant magnetization and γ is a magnetoelastic coupling coefficient.

For regimes in which thermal activation is significant, the local magnetization $\bar{M}$ is specified by Eq. (6) with the

$$[\bar{M}(H,\varepsilon;H_c,\xi)](t)=\begin{cases} [\bar{M}(H,\varepsilon;H_c,\xi)](0), & \tau(t)=\varnothing, \\ \dfrac{H}{\eta-2Y^M\gamma\varepsilon}-\dfrac{M_R\eta}{\eta-2Y^M\gamma\varepsilon}, & \tau(t)\neq\varnothing \text{ and } H[\max\tau(t)]=-H_c, \\ \dfrac{H}{\eta-2Y^M\gamma\varepsilon}+\dfrac{M_R\eta}{\eta-2Y^M\gamma\varepsilon}, & \tau(t)\neq\varnothing \text{ and } H[\max\tau(t)]=H_c, \end{cases} \qquad (22)$$

where $H_c=\eta(M_R-M_I)$, τ is given by Eq. (13), and

$$[\bar{M}(H,\varepsilon;H_c,\xi)](0)=\begin{cases} \dfrac{H}{\eta-2Y^M\gamma\varepsilon}-\dfrac{M_R\eta}{\eta-2Y^M\gamma\varepsilon}, & H(0)\leqslant -H_c, \\ \xi, & -H_c<H(0)<H_c, \\ \dfrac{H}{\eta-2Y^M\gamma\varepsilon}+\dfrac{M_R\eta}{\eta-2Y^M\gamma\varepsilon}, & H(0)\geqslant H_c. \end{cases} \qquad (23)$$

We note that Eqs. (22) and (23) reduce to Eqs. (12) and (14) in the absence of strains.

The elastic constitutive relation is determined from the equilibrium condition,

$$\frac{\partial G}{\partial\varepsilon}=0,$$

which, as indicated in Eq. (3), yields

$$\sigma=\left.\frac{\partial\psi_e}{\partial\varepsilon}\right|_M.$$

The coupled constitutive relations for the undamped magnetostrictive material are then given by

Gibbs energy relation (21) employed in the integrals [Eqs. (9) and (11)]. For the limiting case of negligible thermal activation, which is determined through solution of $\partial G/\partial M=0$, the local magnetization is given by

$$\sigma=Y^M\varepsilon-Y^M\gamma M^2, \qquad (24)$$

$$M(H,\varepsilon)=C\int_0^\infty\int_{-\infty}^\infty \bar{M}(\mathcal{H}+H,\varepsilon;H_c,\xi)$$
$$\times e^{-\mathcal{H}^2/\bar{b}}e^{-(H_c-\bar{H}_c)^2/b}\,d\mathcal{H}\,dH_c,$$

with $\bar{M}$ specified by Eqs. (22) in the absence of thermal activation or Eq. (6) with G given by Eq. (21) when thermal activation, or relaxation mechanisms, are significant.
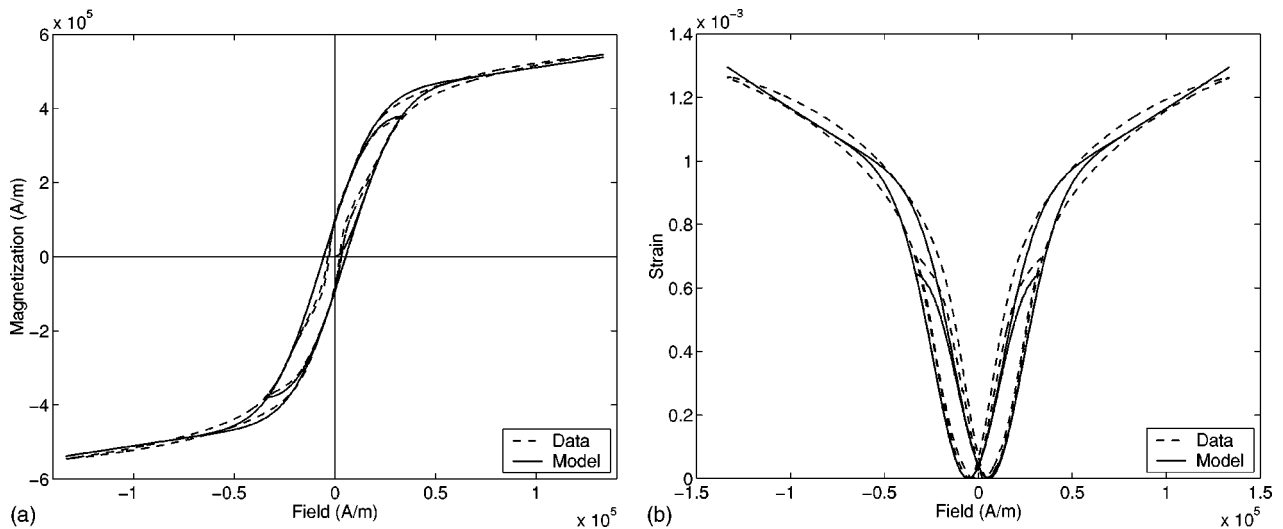

FIG. 8. Experimental data $(---)$ from Ref. 8 and model response (———): (a) field-magnetization relation and (b) field-strain relation.

III. MODEL VALIDATION

To illustrate properties of the model, we present two examples. In the first, the model is used to characterize and predict the magnetization and strains produced by a Terfenol-D transducer. The second illustrates numerically the ability of the model to close biased minor loops.

A. Experimental validation

We first consider the characterization of magnetization and displacements generated by a typical Terfenol-D transducer having the configuration depicted in Fig. 2 in response to a quasistatic input current $I(t)$ to the solenoid. Details regarding the transducer construction and manner through which the experimental data were collected are provided in Ref. 8. We consider here data collected at 1 Hz with a prestress of 1 ksi (6.9 MPa). Two input levels yield the moderate and high drive level magnetization and strain data plotted in Figs. 1 and 8.

The parameters $M_R = 3.7 \times 10^4$ A/m, $\eta = 14$, $H_c = 300$ A/m, $b = 1 \times 10^8$ A^2/m^2, $\bar{b} = 8 \times 10^8$ A^2/m^2, $C = 2.52$

$\times 10^{-8}$, and $\gamma = 4.5 \times 10^{-15}$ m^2/A^2 in relations (24) were estimated through a least squares fit to the high drive level data to produce the model response plotted in Fig. 8. The model with the same parameter values was then used to predict the moderate drive level behavior. Because we considered a fixed prestress regime, we neglected components of the magnetomechanical coupling in constitutive relations (24). Hence the bulk magnetization M was computed using the local magnetization relation (22) with $\varepsilon = 0$ and the magnetostriction $\lambda \equiv \gamma M^2$ was used to model the strains measured.

Although certain discrepancies exist between the modeled magnetization and strains and the experimental measurements, the overall behavior predicted by the model is sufficiently accurate for material characterization and control design. The contraction in the low field magnetization data is typically attributed to crystalline anisotropies inherent to Terfenol-D. The present model does not incorporate anisotropy energy and hence lacks mechanisms necessary to achieve this low field change in concavity. The discrepancy
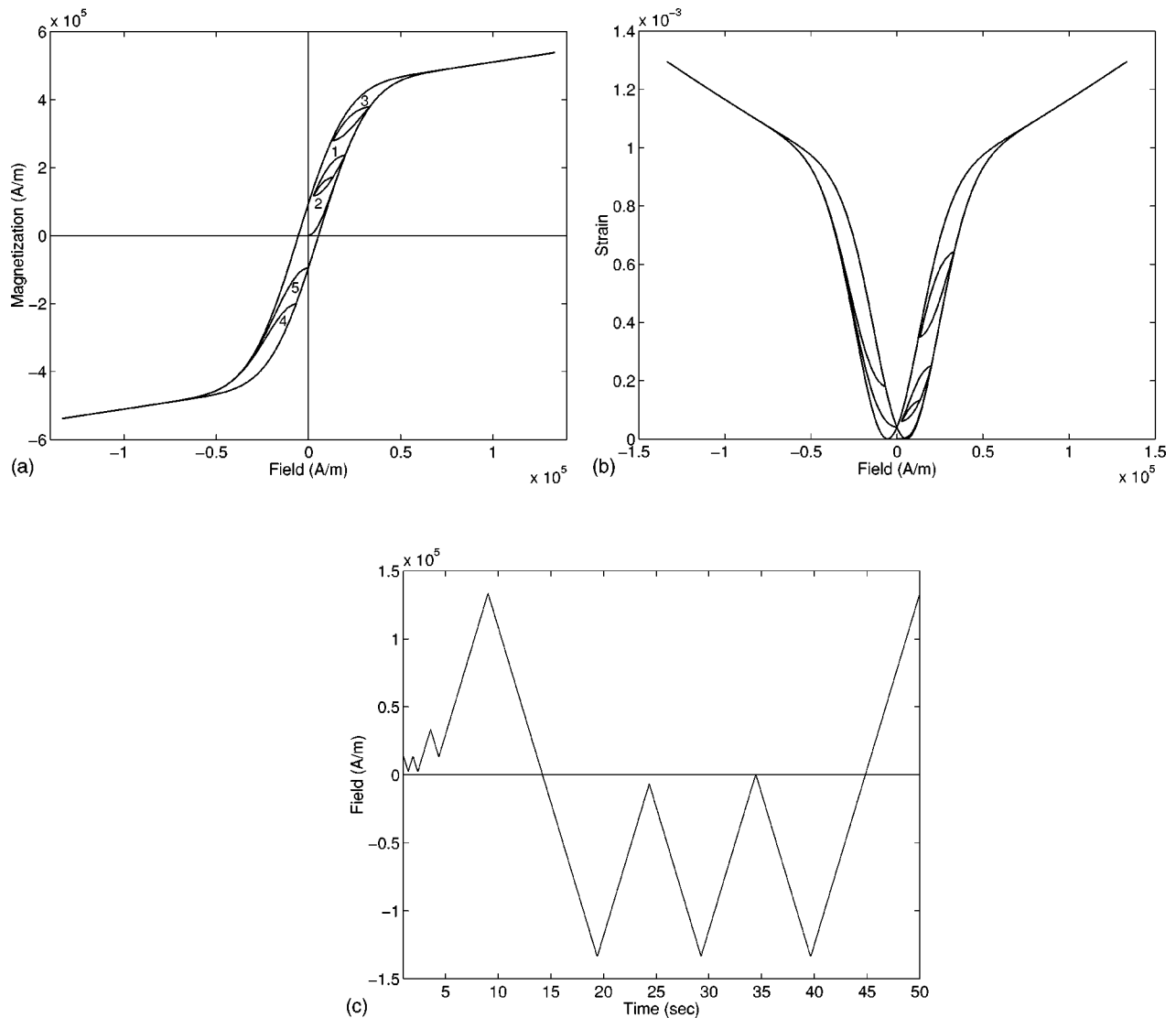

FIG. 9. (a) Magnetization predicted by the model, (b) strains profile predicted by the model, and (c) input field H to the model.

between the model and data in the tips of the strain loop indicates limitations in the quadratic magnetostriction model and potential mechanical coupling which must be incorporated through a partial differential equations (PDE) model for the rod based on constitutive relations (24). The development of a distributed rod model and the computation of total strains and displacements can be addressed in the manner detailed in Refs. 8 and 9.

B. Biased minor loops

To illustrate model properties under asymmetric minor loop operation, the field plotted in Fig. 9(c) was provided as input to the model which yielded the magnetization and strain responses plotted in Figs. 9(a) and 9(b). The parameters in the model were taken to be those specified in the example in Sec. III A which were obtained through a least squares fit to high drive level data. Loops 1 and 3 illustrate biased minor loop behavior while loop 2 illustrates the ability of the model to enforce closure of multiply nested minor loops. Loops 4 and 5 illustrate biased behavior leading to saturation. When combined with the experimental results presented in Sec. III A, the behavior illustrated here provides the model with substantial flexibility for material characterization and control design.

IV. CONCLUDING REMARKS

In this article we presented a model theory which quantifies hysteresis and constitutive nonlinearities in magnetostrictive transducers operating in moderate to high drive regimes. By combining free energy analysis at the lattice or domain level with stochastic distributions to accommodate material and field nonhomogeneities, we obtain a low-order macroscopic model that automatically ensures the closure of biased, nested, minor loops. In its present form, the model incorporates relaxation mechanisms but neglects eddy current losses so, to avoid simulation inaccuracies, it should be restricted to low frequencies of operation. Errors introduced by employing the model at high frequencies include phase shifts and overestimation of magnetization values. Additionally, although stress or strain effects have been included in the free energy formulations, the accuracy of the model for quantifying full magnetoelastic coupling has not yet been established. As indicated in Sec. III, this will involve in part the formulation of a PDE model for the Terfenol-*D* rod and subsequent Galerkin or finite element discretization to obtain a finite dimensional model. The model also neglects self-heating in the transducer as well as crystalline anisotropy. A number of present transducer designs employ water cooling to maintain approximately isothermal conditions and require prestress levels at which stress anisotropy dominate crystalline anisotropy. For these regimes, the model accurately quantifies the low frequency dynamics of the transducer.

We note that the free energy framework for this model originated in the context of shape memory alloys (SMA)[19,20] and was recently extended to piezoceramic compounds[21]

where a distributional analysis concerning variable coercive and effective fields was added. Hence the theory provides a unified framework for modeling hysteresis in a number of representative smart material systems. Furthermore, it was illustrated in Ref. 18 that the framework can be employed to provide an energy basis for Preisach models with the following important difference: temperature and relaxation dependencies are manifested in the kernel or basis for this model whereas they enter the parameters, or measures, in Preisach expansions. This has important consequences for control design since it provides the potential for eliminating the gain scheduling required to accommodate changing parameters in broadband control regimes or systems with fluctuating temperatures.

[1] M. J. Dapino, in *Encyclopedia of Smart Materials*, edited by M. Schwartz (Wiley, New York, to be published).
[2] M. J. Dapino, F. T. Calkins, and A. B. Flatau, in *Wiley Encyclopedia of Electrical and Electronics Engineering*, edited by J. G. Webster (Wiley, New York, 1999), Vol. 12, p. 278.
[3] J. B. Restorff, Encycl. Appl. Phys. **9**, 229 (1994).
[4] M. Wun-Fogle, J. B. Restorff, A. E. Clark, and J. F. Lindberg, J. Appl. Phys. **83**, 7279 (1998).
[5] J. B. Restorff, H. T. Savage, A. E. Clark, and M. Wun-Fogle, J. Appl. Phys. **67**, 5016 (1996).
[6] R. C. Smith, J. Math. Syst. Estim. Control **8**, 249 (1998).
[7] F. T. Calkins, R. C. Smith, and A. B. Flatau, IEEE Trans. Magn. **36**, 429 (2000).
[8] M. J. Dapino, R. C. Smith, L. E. Faidley, and A. B. Flatau, J. Intell. Mater. Syst. Struct. **11**, 134 (2000).
[9] M. J. Dapino, R. C. Smith, and A. B. Flatau, IEEE Trans. Magn. **36**, 545 (2000).
[10] D. C. Jiles, *Introduction to Magnetism and Magnetic Materials* (Chapman and Hall, New York, 1991).
[11] D. C. Jiles and D. L. Atherton, J. Magn. Magn. Mater. **61**, 48 (1986).
[12] E. Della Torre, *Magnetic Hysteresis* (IEEE, New York, 1999).
[13] F. Liorzou, B. Phelps, and D. L. Atherton, IEEE Trans. Magn. **36**, 418 (2000).
[14] K. H. Carpenter, IEEE Trans. Magn. **26**, 4404 (1991).
[15] D. C. Jiles, IEEE Trans. Magn. **28**, 2602 (1992).
[16] R. C. Smith and J. E. Massad, *Proceedings of the 18th ASME Biennial Conference on Mechanical Vibration and Noise*, 2001.
[17] B. D. Cullity, *Introduction to Magnetic Materials* (Addison–Wesley, Reading, MA, 1972).
[18] R. C. Smith and S. Seelecke, in Ref. 21, p. 4693.
[19] N. Papenfuss and S. Seelecke, *SPIE Smart Structures and Materials* (Mathematics and Control in Smart Structures, San Diego, CA, 1999), p. 586.
[20] S. Seelecke and C. Büskens, in *Computer Aided Optimum Design of Structures*, edited by V. S. Hernández and C. A. Brebbia (Computational Mechanics, 1997), p. 457.
[21] R. C. Smith, S. Seelecke, and Z. Ounaies, in *SPIE Smart Structures and Materials* (Modeling, Signal Processing and Control, San Diego, CA, 2002), p. 4693.